Computer Methods in Biomechanics and Biomedical Engineering

ISSN: 1025-5842 (Print) 1476-8259 (Online) Journal homepage: https://www.tandfonline.com/loi/gcmb20

Shape optimization in steady blood flow: A numerical study of non-Newtonian effects

Feby Abraham , Marek Behr & Matthias Heinkenschloss

To cite this article: Feby Abraham , Marek Behr & Matthias Heinkenschloss (2005) Shape optimization in steady blood flow: A numerical study of non-Newtonian effects, Computer Methods in Biomechanics and Biomedical Engineering, 8:2, 127-137, DOI: 10.1080/10255840500180799

To link to this article: https://doi.org/10.1080/10255840500180799

Published online: 19 Aug 2006.

Computer Methods in Biomechanics and Biomedical Engineering,
Vol. 8, No. 2, April 2005, 127–137

Taylor & Francis
Taylor & Francis Group

Shape optimization in steady blood flow: A numerical study of non-Newtonian effects

FEBY ABRAHAM†, MAREK BEHR‡* and MATTHIAS HEINKENSCHLOSS¶

†Mechanical Engineering and Applied Mechanics, University of Pennsylvania, Philadelphia, PA 19104, USA
‡Chair for Computational Analysis of Technical Systems, CCES, RWTH Aachen University, 52056 Aachen, Germany
¶Computational and Applied Mathematics, Rice University - MS 134, 6100 Main Street, Houston, TX 77005, USA

(Received 9 February 2004; in final form 5 May 2005)

We investigate the influence of the fluid constitutive model on the outcome of shape optimization tasks, motivated by optimal design problems in biomedical engineering. Our computations are based on the Navier-Stokes equations generalized to non-Newtonian fluid, with the modified Cross model employed to account for the shear-thinning behavior of blood. The generalized Newtonian treatment exhibits striking differences in the velocity field for smaller shear rates. We apply sensitivity-based optimization procedure to a flow through an idealized arterial graft. For this problem we study the influence of the inflow velocity, and thus the shear rate. Furthermore, we introduce an additional factor in the form of a geometric parameter, and study its effect on the optimal shape obtained.

Keywords: Shape optimization; Blood flow; Non-Newtonian fluids; Navier-Stokes equations

1. Introduction

The use of computational fluid dynamics (CFD) in the study of physiological flows involving blood is an area of intensive research. Part of the challenge in this field is the accurate treatment of the haemodynamic behaviour—see, e.g. Quarteroni *et al.* (2000) for a recent review in this field. A variety of models have been proposed that capture the viscoelastic and shear-thinning behaviour of blood. The papers of Yeleswarapu (1996), Gijsen *et al.* (1999), Leuprecht and Perktold (2001), Neofytou and Drikakis (2003) and Johnston *et al.* (2004) provide a small sample of the research on non-Newtonian effects on blood flow. A less-studied area is the usage of numerical optimization procedures to guide the design process that involves blood flow. CFD-based numerical optimization procedures far outperform traditional trial and error methods in the evaluation of design decisions, in terms of robustness, cost and automation of the entire process.

Given a partial differential equation (PDE) model of the flow, shape optimization aims to extremize a given objective—subject to physical or geometric constraints—through the variation of the domain or a part of it. Such problems arise in a multitude of engineering applications. Shape optimization procedures have been extensively studied in the context of aerodynamic flows (Mohammadi and Pironneau 2001, Gunzburger 2003), and there has been recent interest to extend these successes, to biomedical applications (Antaki *et al.* 1995, He *et al.* 1997, Burgreen *et al.* 2001, Quarteroni and Rozza 2003). In the latter references, a Newtonian model is used to represent the blood flow.

This paper presents a numerical study of non-Newtonian effects on the solution of shape optimization problems for an idealized biomedical system. Our work is motivated by the desire to find optimal shapes in the context of continuous-flow centrifugal blood pumps (Behr and Arora 2003), which are being intensively studied as a bridge to transplant, or with enough technological maturity, as a long-term autonomous artificial heart. Our current study is a step in this direction. To account for the shear-thinning behaviour of blood, we make use of generalized Newtonian constitutive equations of the modified Cross model, e.g. Leuprecht and Perktold (2001). A Newtonian assumption is generally considered valid for flows where shear rates are high, thus diminishing the shear-related viscosity differences. Gijsen *et al.* (1999) show higher differences in the axial velocity profile compared to results obtained by Perktold *et al.* (1991) for a 3D carotid bifurcation study when using

*Corresponding author. E-mail: behr@cats.rwth-aachen.de

Computer Methods in Biomechanics and Biomedical Engineering
ISSN 1025-5842 print/ISSN 1476-8259 online © 2005 Taylor & Francis Group Ltd
http://www.tandf.co.uk/journals
DOI: 10.1080/10255840500180799

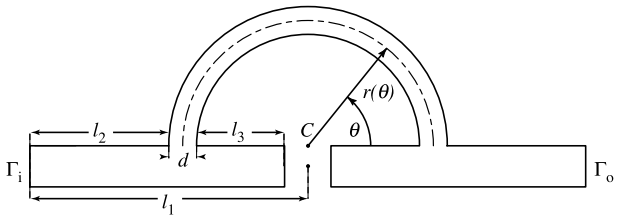

Figure 1. Computational domain for the arterial graft. The initial shape of the design curve of the graft (dashed line) is a semi-circle with center at C. Fixed geometry parameters are $l_1 = 6.0$, $l_2 = 3.0$, $l_3 + d = 2.5$. The downstream section of the host artery is symmetric with respect to the upstream one.

lower mean axial velocity and a larger diameter of the carotid artery, which results in a lower shear rate.

We examine an idealized bypass graft, commonly used as an alternative route around critically stenosed arteries. Specifically, we study a model with a complete stenosis, one that precludes any flow between the proximal and distal end of the host artery. Guo *et al.* (2001) study the effect of graft placement vis-a-vis the occlusion as an important criterion for improving the outcome of coronary artery bypass grafting. Favourable graft angle (Grad and Einav 1998, Quarteroni and Rozza 2003), as well as graft-to-artery ratio and graft hood shape, have also been identified as factors that can ensure favourable flow, which then precludes the development of further occlusions. Quarteroni and Rozza (2003) recently studied optimal design in the context of prosthetic grafting using Newtonian constitutive equations. The design is computed using a lower fidelity Stokes equation. The computed shape is then tested for suitable design control quantities defined over the more expensive unsteady Navier-Stokes flow solution. In Abraham (2004), we have also considered the shape optimization of a two-dimensional inflow cannula of a circulatory assist device, previously studied by He *et al.* (1997) using Newtonian constitutive equations.

The governing equations for the fluid flow and a model shape optimization problem are described in the second section. For the numerical solution of the shape optimization problem we discretize the Navier-Stokes equation using Galerkin/Least-Squares (GLS) stabilized piecewise-linear finite elements. The discretized shape optimization problem is solved using a gradient-based optimization algorithm. The details of the finite element discretization of the problem, computation of derivatives in our optimization problem as well as specifications of the optimization algorithm used is given in the third section. The fourth section reports on the numerical results for our test case.

2. A model shape optimization problem

We first introduce the equations for blood flow in a fixed domain $\Omega \subset \mathbb{R}^{n_{\rm sd}}$, where $n_{\rm sd}$ is the number of space dimensions. The symbols $\mathbf{u}$ and p represent the velocity and pressure. The boundary $\partial\Omega$ of Ω is decomposed into two disjoint segments Γ_h and Γ_g. The momentum and mass balance equations subject to Neumann and Dirichlet boundary conditions, can be written as

$$\begin{aligned} \rho(\mathbf{u}\cdot\nabla\mathbf{u}) - \nabla\cdot\boldsymbol{\sigma}(\mathbf{u},p) = 0 \quad &\text{on } \Omega, \\ \nabla\cdot\mathbf{u} = 0 \quad &\text{on } \Omega, \\ \mathbf{n}\cdot\boldsymbol{\sigma}(\mathbf{u},p) = h \quad &\text{on } \Gamma_h, \\ \mathbf{u} = g \quad &\text{on } \Gamma_g. \end{aligned} \tag{1}$$

The stress tensor $\boldsymbol{\sigma}$ is given by

$$\boldsymbol{\sigma}(\mathbf{u},p) = -p\mathbf{I} + 2\mu\varepsilon(\mathbf{u}), \quad \varepsilon(\mathbf{u}) = \frac{1}{2}(\nabla\mathbf{u} + \nabla\mathbf{u}^T), \tag{2}$$

where μ is the dynamic viscosity, ρ is the density and $\mathbf{I}$ denotes the identity tensor. For a Newtonian fluid μ is a constant, whereas in the case of a generalized Newtonian fluid, we incorporate the shear-thinning

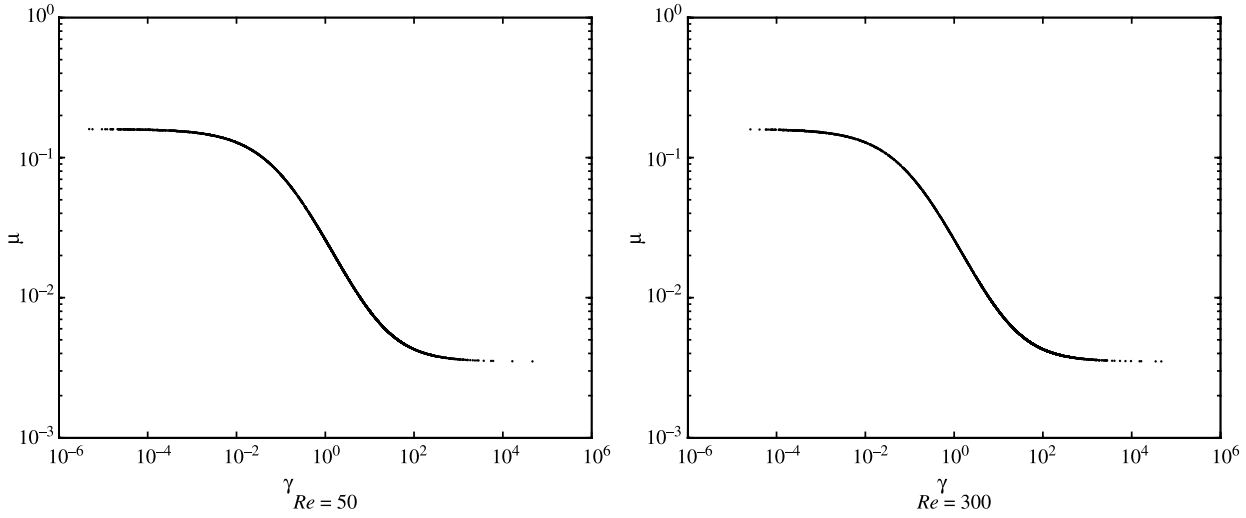

Figure 2. The viscosity and corresponding shear rate profile for the initial shape of the graft geometry for case 1, using the modified Cross constitutive equation for $Re = 50$ (left) and $Re = 300$ (right).

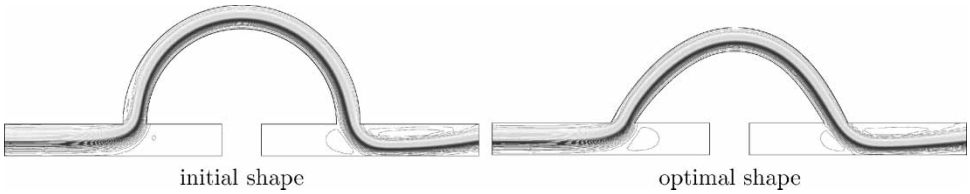

Figure 3. The graft streamline velocity profile for the initial and the optimal shape, using the Newtonian constitutive equation for case 1, $Re = 300$.

behaviour of blood, as expressed by the modifed Cross model:

$$\mu(\dot{\gamma}) = \mu_\infty + \frac{\mu_0 - \mu_\infty}{(1 + (\lambda\gamma)^b)^a}. \tag{3}$$

Here, μ_∞ and μ_0 are the infinite shear viscosity and the zero shear viscosity, respectively. The parameter values follow (Leuprecht and Perktold 2001): $\mu_\infty = 0.0035\,\text{Pa s}$, $\mu_0 = 0.1600\,\text{Pa s}$, $\lambda = 8.2\,\text{s}$, $a = 1.23$ and $b = 0.64$. For general flows, the scalar shear rate is computed using the second invariant of the symmetric rate-of-deformation tensor

$$\gamma = \sqrt{2\varepsilon(\mathbf{u}) : \varepsilon(\mathbf{u})}. \tag{4}$$

The fluid density is taken as $\rho = 1.058\,\text{g/cm}^3$. We note that the modified Cross model is equivalent to the Carreau-Yasuda model (Yeleswarapu 1996, Gijsen *et al.* 1999, Leuprecht and Perktold 2001) provided that the parameters in both models are properly related.

For the differential equation described in equation (1), a weak form is constructed as follows. We define the function spaces

$$\begin{aligned} \mathcal{S} &= \{\mathbf{u} | \mathbf{u} \in [H^1(\Omega)]^{n_{\text{sd}}}, \quad \mathbf{u} = g \quad \text{on} \quad \Gamma_g\}, \\ \mathcal{V} &= \{\mathbf{u} | \mathbf{u} \in [H^1(\Omega)]^{n_{\text{sd}}}, \quad \mathbf{u} = 0 \quad \text{on} \quad \Gamma_g\}, \end{aligned}$$

where $H^1(\Omega)$ is defined in the usual way (Girault and Raviart 1986, Gunzburger 1989). The weak form of equation (1) is to find $\mathbf{u} \in \mathcal{S}_\mathbf{u}$ and $p \in L^2(\Omega)$, such that

$$\begin{aligned} \int_\Omega \mathbf{w}\cdot\rho(\mathbf{u}\cdot\nabla\mathbf{u})\,\mathrm{d}\mathbf{x} + \int_\Omega \varepsilon(\mathbf{w}) : \boldsymbol{\sigma}(\mathbf{u}, p)\,\mathrm{d}\mathbf{x} + \\ \int_\Omega q\nabla\cdot\mathbf{u}\,\mathrm{d}\mathbf{x} = \int_{\Gamma_h} \mathbf{w}\cdot h\,\mathrm{d}\mathbf{x} \end{aligned} \tag{5}$$

for all $\mathbf{w} \in \mathcal{V}$ and for all $q \in L^2(\Omega)$.

Our goal is to find a shape Ω such that a given objective function J, which depends on $\mathbf{u}$, p and on Ω, is minimized. We consider the case where the set of admissible shapes can be parameterized by $\boldsymbol{\alpha} \in \mathcal{A}_{\text{ad}} \subset \mathbb{R}^n$. The optimal shape design problem is given as follows.

$$\begin{aligned} &\text{Minimize} \quad J(\mathbf{u}, p, \boldsymbol{\alpha}), \\ &\text{subject to} \quad (5) \quad \text{with} \quad \Omega = \Omega(\boldsymbol{\alpha}), \\ &\qquad\qquad \boldsymbol{\alpha} \in \mathcal{A}_{\text{ad}}. \end{aligned} \tag{6}$$

A critical criterion for design decisions involving blood, such as for those involving prosthetic devices or artificial heart components, is to minimize the mechanical loading on blood particles, which is related to the shear stress in the flow field. Processes such as the damage of red blood cells (hemolysis), platelet aggregation and thrombus formation on artificial surfaces, are all influenced by the shear stress, making it a quantity of significant clinical importance (He *et al.* 1997, Grigioni *et al.* 2002). Therefore, we use the integral of the squared shear rate in our computations, i.e.

$$J(\mathbf{u}, p, \boldsymbol{\alpha}) = 2\int_{\Omega_{\text{obs}}(\boldsymbol{\alpha})} \varepsilon(\mathbf{u}) : \varepsilon(\mathbf{u})\,\mathrm{d}\mathbf{x}, \tag{7}$$

where $\Omega_{\text{obs}}(\boldsymbol{\alpha}) \subset \Omega(\boldsymbol{\alpha})$, represents the observation region. We also refer to equation (7) as the dissipation function. Note that in the case of equation (7), J only depends on $\mathbf{u}$ but not (explicitly) on p,$\boldsymbol{\alpha}$.

3. Numerical solution of the optimization problem

3.1 Discretization of the optimization problem

To discretize the governing equations (5), we apply a stabilized finite element discretization using conforming piecewise linear finite elements for the velocities and the pressure. Let $\{\Omega^e(\boldsymbol{\alpha}) | \, e = 1, 2, \ldots, n_{\text{el}}\}$ be a triangulation

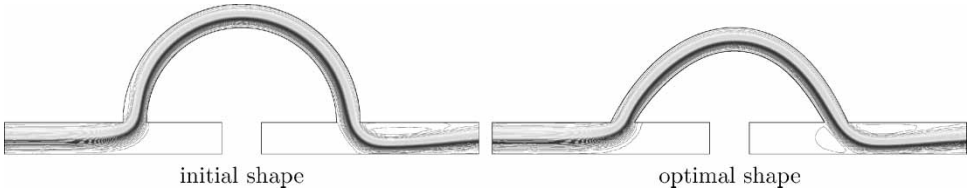

Figure 4. The graft streamline velocity profile for the initial and the optimal shape, using the modified Cross constitutive model for case 1, $Re = 300$.

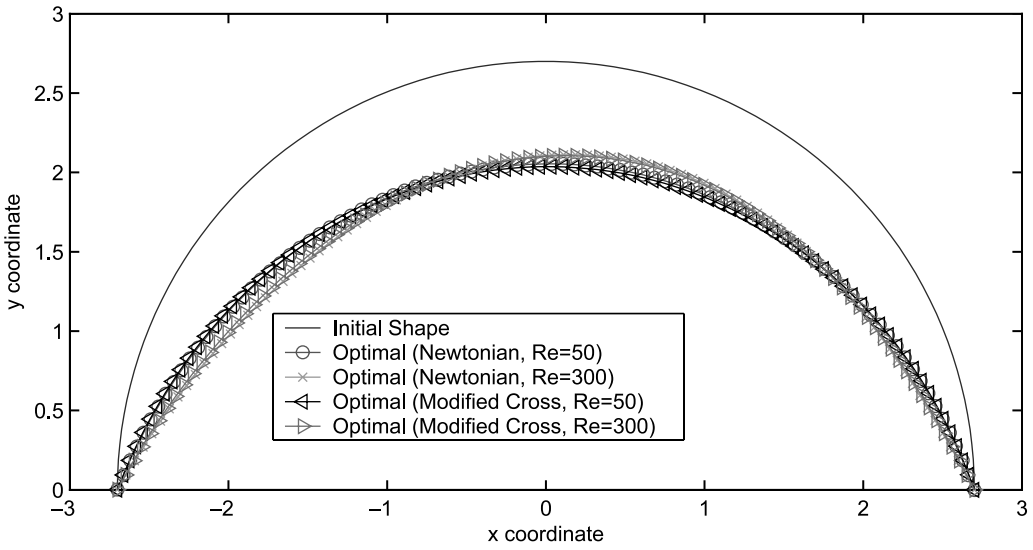

Figure 5. Initial shape and optimal shape of the graft design curve for the Newtonian and modified Cross constitutive model, $d = 0.6$.

of $\Omega(\boldsymbol{\alpha})$. We set

$$H^{1h}(\Omega(\boldsymbol{\alpha})) = \{v \in C(\Omega(\boldsymbol{\alpha}))|v \text{ is linear on } \Omega^e(\boldsymbol{\alpha}), \quad e = 1, 2, \ldots, n_{\text{el}}\},$$

$$\mathcal{S}^h = \{\mathbf{u}^h|\mathbf{u}^h \in [H^{1h}(\Omega(\boldsymbol{\alpha}))]^{n_{\text{sd}}}, \quad \mathbf{u}^h = g^h \quad \text{on} \quad \Gamma_g(\boldsymbol{\alpha})\},$$

$$\mathcal{V}^h = \{\mathbf{u}^h|\mathbf{u}^h \in [H^{1h}(\Omega(\boldsymbol{\alpha}))]^{n_{\text{sd}}}, \quad \mathbf{u}^h = 0 \quad \text{on} \quad \Gamma_g(\boldsymbol{\alpha})\}.$$

The GLS stabilized finite element discretization of equation (5) is given as follows. Find $\mathbf{u}^h \in \mathcal{S}^h$ and $p^h \in H^{1h}(\Omega(\boldsymbol{\alpha}))$, such that

$$\int_{\Omega(\boldsymbol{\alpha})} \mathbf{w}^h \cdot \rho(\mathbf{u}^h \cdot \nabla \mathbf{u}^h)\,d\mathbf{x}^h + \int_{\Omega(\boldsymbol{\alpha})} \boldsymbol{\varepsilon}(\mathbf{w}^h) : \boldsymbol{\sigma}(\mathbf{u}^h, p^h)\,d\mathbf{x}^h + \sum_{e=1}^{n_{\text{el}}} \int_{\Omega^e(\boldsymbol{\alpha})} \tau_{\text{MOM}} \frac{1}{\rho}[\rho(\mathbf{u}^h \cdot \nabla \mathbf{w}^h) - \nabla \cdot \boldsymbol{\sigma}(\mathbf{w}^h, q^h)] \cdot [\rho(\mathbf{u}^h \cdot \nabla \mathbf{u}^h) - \nabla \cdot \boldsymbol{\sigma}(\mathbf{u}^h, p^h)]\,d\mathbf{x}^h + \int_{\Omega(\boldsymbol{\alpha})} q^h \nabla \cdot \mathbf{u}^h\,d\mathbf{x}^h = \int_{\Gamma_h(\boldsymbol{\alpha})} \mathbf{w}^h \cdot h^h\,d\mathbf{x}^h \tag{8}$$

for all $\mathbf{u}^h \in \mathcal{V}^h$ and for all $q^h \in H^{1h}(\Omega(\boldsymbol{\alpha}))$. The GLS stabilization (Shakib 1988, Hughes *et al.* 1989, Tezduyar *et al.* 1992) provides stability at high element-level Reynolds numbers and circumvents the LBB (inf–sup) condition. In particular, it allows the use of piecewise linear functions to approximate both the velocity and the pressure. The coefficient for the GLS stabilization, τ_{MOM}, in equation (8) is defined, e.g. in Shakib (1988). It depends on the element length h_e, which in our computations is specified by the `adv` definition in Abraham *et al.* (2004).

Since we use piecewise linear functions, the second derivatives arising in the computation of $\nabla \cdot \boldsymbol{\sigma}(\mathbf{u}^h, p^h)$ on $\Omega^e(\boldsymbol{\alpha})$ are zero. Our implementation of equation (8) replaces $\nabla \cdot \boldsymbol{\sigma}(\mathbf{w}^h, q^h)$, $\nabla \cdot \boldsymbol{\sigma}(\mathbf{u}^h, p^h)$ by $-\nabla q^h$, $-\nabla p^h$, respectively. As a consequence, our stabilized finite element formulation is only "weakly consistent". A variational reconstruction of second derivatives (Jansen *et al.* 1999) could be used to improve the consistency of our approximation.

Let $\mathbf{x}^h(\boldsymbol{\alpha}) \in \Omega(\boldsymbol{\alpha})$ denote the nodes associated with the nodal basis for $H^{1h}(\Omega(\boldsymbol{\alpha}))$. We can represent equation (8) symbolically as

$$\mathbf{c}^h(\mathbf{u}^h(\boldsymbol{\alpha}), p^h(\boldsymbol{\alpha}), \mathbf{x}^h(\boldsymbol{\alpha})) = 0. \tag{9}$$

We assume that for any $\boldsymbol{\alpha} \in \mathcal{A}_{\text{ad}}$ the equation (9) has a unique solution $\mathbf{u}^h(\boldsymbol{\alpha}), p^h(\boldsymbol{\alpha})$. We compute an approximation of this solution using an Newton GMRES method (Kelley 1995).

Remark 3.1. The second term in equation (8) contains $\int_{\Omega(\boldsymbol{\alpha})} \boldsymbol{\varepsilon}(\mathbf{w}^h) : 2\mu\boldsymbol{\varepsilon}(\mathbf{u}^h)\,d\mathbf{x}^h$. When the modified Cross model is used, μ depends on $\mathbf{u}$ (cf. equations (3) and (4)).

Table 1. The design variables for the graft optimization for case 1, $Re = 300$.

Design variable	Initial	Newtonian	Modified Cross
r_2	0.0	1.703	1.529
r_3	0.0	−1.013	−0.880
r_4	0.0	0.265	0.228
r_5	0.0	−0.022	−0.018

Table 2. The angle that the graft makes with the artery for case 1.

Angle	Initial	Newtonian	Modified Cross
$\theta = 0$, $Re = 50$	90.00°	69.70°	70.81°
$\theta = \pi$, $Re = 50$	90.00°	68.21°	68.92°
$\theta = 0$, $Re = 300$	90.00°	61.78°	62.89°
$\theta = \pi$, $Re = 300$	90.00°	60.86°	62.15°

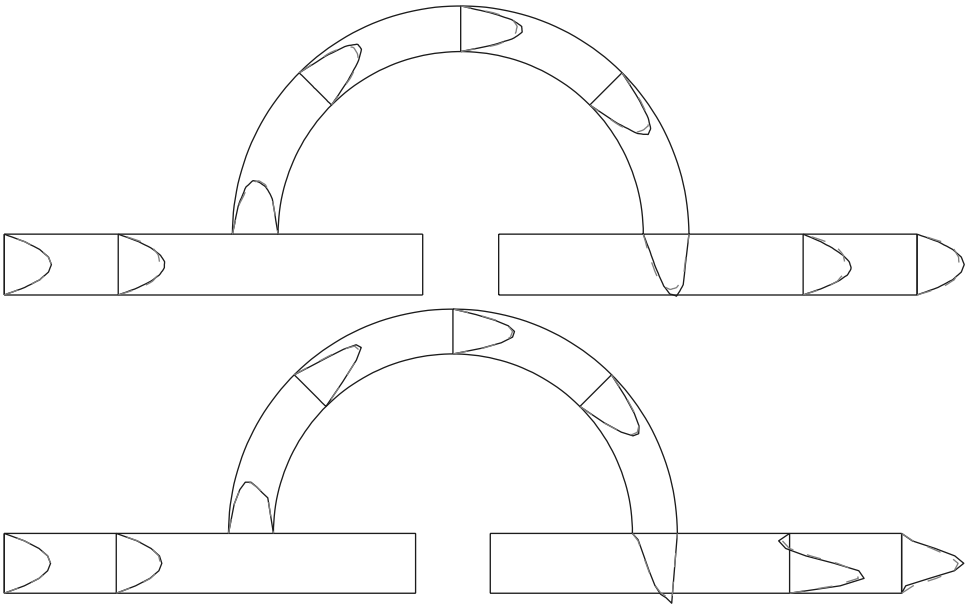

Figure 6. Axial velocity plot at various locations of the initial graft shape, for case 1, with $Re = 50$ (top) and $Re = 300$ (bottom). Solid line represents Newtonian flow and dashed line represents the flow using the modified Cross constitutive model. The velocities in the top subplot are scaled by a factor of 6 relative to the bottom subplot to emphasize differences in downstream velocity profiles.

In this case, the evaluation of $\partial \mathbf{c}^h / \partial \mathbf{u}^h$ requires us to compute the derivative of μ with respect to $\mathbf{u}^{\mathrm{h}}$. In our computations we drop this derivative. This leads to an inexactness in the Jacobian $\partial \mathbf{c}^h / \partial \mathbf{u}^h$. While this inexact Jacobian may effect the convergence of the Newton GMRES method, we have found the performance of our Newton GMRES method satisfactory, and we, therefore, choose to avoid the additional implementation effort required to compute the exact Jacobian $\partial \mathbf{c}^h / \partial \mathbf{u}^h$.

The discretized shape optimization problem may now be written as

$$\begin{aligned} &\text{Minimize} \quad \hat{J}^h(\boldsymbol{\alpha}), \\ &\text{subject to } \boldsymbol{\alpha} \in \mathcal{A}_{\mathrm{ad}}, \end{aligned} \tag{10}$$

where

$$\hat{J}^h(\boldsymbol{\alpha}) = J^h(\mathbf{u}^h(\boldsymbol{\alpha}), p^h(\boldsymbol{\alpha}), \mathbf{x}^h(\boldsymbol{\alpha}), \boldsymbol{\alpha}).$$

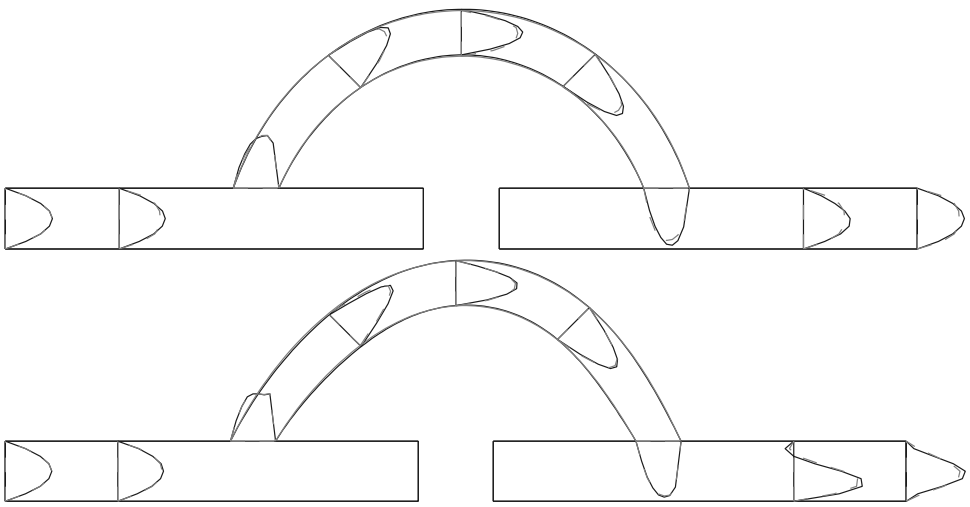

Figure 7. Axial velocity plot at various locations of the optimal graft shapes using each of the constitutive equation (overlapped here), for case 1, with $Re = 50$ (top) and $Re = 300$ (bottom). Solid line represents Newtonian flow and dashed line represents the flow using the modified Cross constitutive model. The velocities in the top subplot are scaled by a factor of 6 relative to the bottom subplot to emphasize differences in downstream velocity profiles.

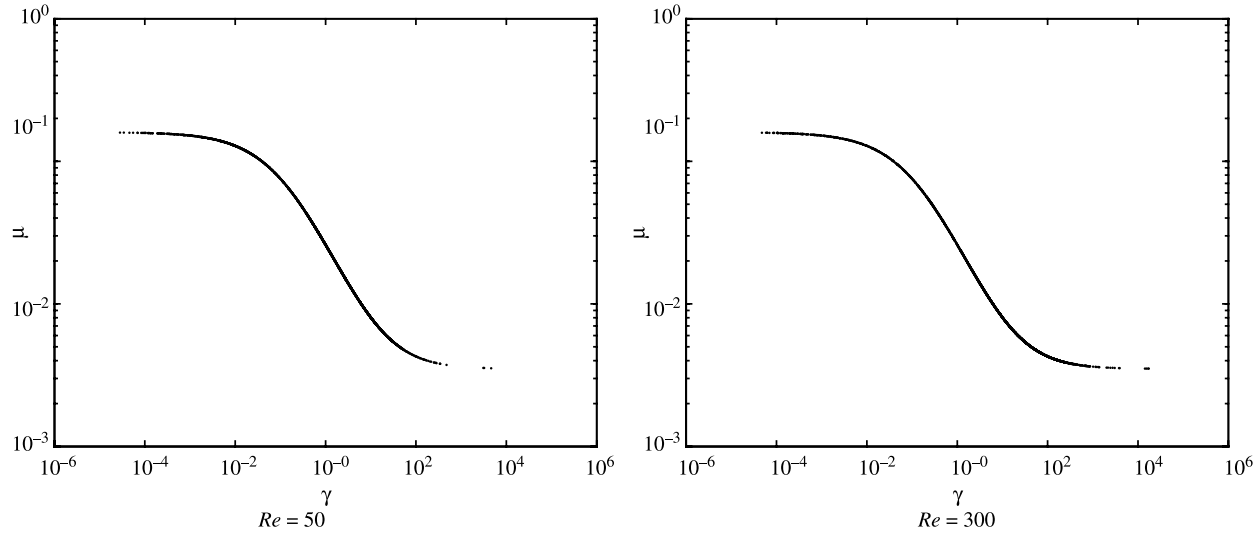

Figure 8. The viscosity and corresponding shear rate profile for the initial shape of the graft geometry for case 2, using the modified Cross constitutive equation for $Re = 50$ (left) and $Re = 300$ (right).

Note that in equation (10), the velocities and pressure, $\mathbf{u}^h(\boldsymbol{\alpha})$ and $p^h(\boldsymbol{\alpha})$, are implicit functions of the design parameter $\boldsymbol{\alpha}$. These implicit functions are defined as the solution of equation (9). This is referred to as the black-box or nested analysis and design (NAND) approach.

In equation (6), the velocities and pressures as well as the design parameters $\boldsymbol{\alpha}$ are optimization variables. The velocities and pressures are coupled to the design parameters $\boldsymbol{\alpha}$ through the governing equation, which in equation (6) is included as an explicit constraint. This is referred to as the all-at-once or simultaneous analysis and design (SAND) approach. The SAND approach could have also been used for the formulation of the discretized problem. The formulation of the optimization problem and the associated optimization algorithm can have a great impact on the efficiency with which the problem can be solved. In particular, SAND formulations combined with sequential quadratic programming (SQP) methods are very attractive. For the purpose of this paper, however, the efficiency with which the optimization problem equation (10) is solved is secondary. Our optimization is built onto an existing complex flow code. Since SAND formulations combined with SQP methods require more code modifications than the gradient-based method we use to solve equation (10), we have chosen the latter.

3.2 Gradient computation

We use a gradient-based algorithm to solve the problem (10). Note that the design variables $\boldsymbol{\alpha}$ enter $\hat{J}^h$ explicitly as well as implicitly through $\mathbf{v}^h = (\mathbf{u}^h, p^h)$ and $\mathbf{x}^h$. Hence, the gradient of $\hat{J}^h$ with respect to $\boldsymbol{\alpha}$ is given by

$$\nabla \hat{J}^h = \frac{\partial J^h}{\partial \boldsymbol{\alpha}} + \frac{\partial J^h}{\partial \mathbf{x}^h}\frac{\mathrm{d}\mathbf{x}^h}{\mathrm{d}\boldsymbol{\alpha}} + \frac{\partial J^h}{\partial \mathbf{v}^h}\frac{\mathrm{d}\mathbf{v}^h}{\mathrm{d}\boldsymbol{\alpha}}. \tag{11}$$

The Jacobian of the state variables $\mathbf{v}^h = (\mathbf{u}^h, p^h)$ with respect to $\boldsymbol{\alpha}$ can now be obtained using the implicit function theorem applied to equation (9). This gives

$$\frac{\partial \mathbf{c}}{\partial \mathbf{v}^h}\frac{\mathrm{d}\mathbf{v}^h}{\mathrm{d}\boldsymbol{\alpha}} + \frac{\partial \mathbf{c}}{\partial \mathbf{x}^h}\frac{\mathrm{d}\mathbf{x}^h}{\mathrm{d}\boldsymbol{\alpha}} = 0. \tag{12}$$

Equation (12) is referred to as the discrete sensitivity equation.

Using equation (12) in equation (11), we get

$$\nabla \hat{J}^h = \frac{\partial J^h}{\partial \boldsymbol{\alpha}} + \frac{\partial J^h}{\partial \mathbf{x}^h}\frac{\mathrm{d}\mathbf{x}^h}{\mathrm{d}\boldsymbol{\alpha}} - \frac{\partial J^h}{\partial \mathbf{v}^h}\left[\left(\frac{\partial \mathbf{c}}{\partial \mathbf{v}^h}\right)^{-1}\frac{\partial \mathbf{c}}{\partial \mathbf{x}^h}\frac{\mathrm{d}\mathbf{x}^h}{\mathrm{d}\boldsymbol{\alpha}}\right], \tag{13}$$

$$= \frac{\partial J}{\partial \boldsymbol{\alpha}} + \frac{\partial J}{\partial \mathbf{x}^h}\frac{\mathrm{d}\mathbf{x}^h}{\mathrm{d}\boldsymbol{\alpha}} - \left[\left(\frac{\partial \mathbf{c}}{\partial \mathbf{v}^h}\right)^{-1}\frac{\partial J}{\partial \mathbf{v}^h}\right]^T\frac{\partial \mathbf{c}}{\partial \mathbf{x}^h}\frac{\mathrm{d}\mathbf{x}^h}{\mathrm{d}\boldsymbol{\alpha}}. \tag{14}$$

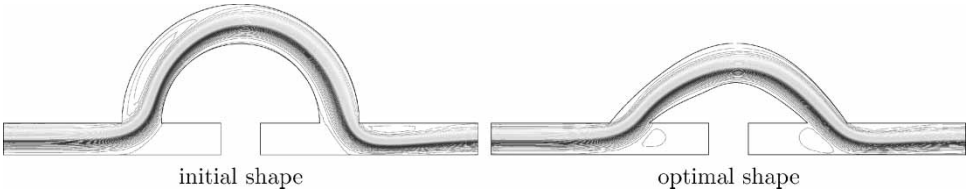

Figure 9. The graft streamline velocity profile for the initial and the optimal shape, using the Newtonian constitutive equation for case 2, $Re = 300$.

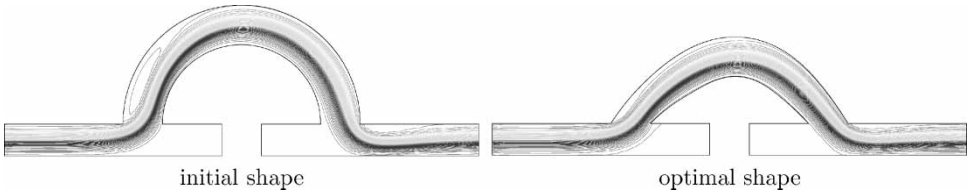

Figure 10. The graft streamline velocity profile for the initial and the optimal shape, using the Newtonian constitutive equation for case 2, $Re = 300$.

To compute the derivatives in case of the sensitivity approach, one forms

$$\left[\left(\frac{\partial \mathbf{c}}{\partial \mathbf{v}^h}\right)^{-1}\frac{\partial \mathbf{c}}{\partial \mathbf{x}^h}\frac{\mathrm{d}\mathbf{x}^h}{d\alpha}\right]$$

for each α_i and computes the derivative from equation (13) for each of the n design variables. In another approach, known as the adjoint approach, one forms

$$\left[\left(\frac{\partial \mathbf{c}}{\partial \mathbf{v}^h}\right)^{-1}\frac{\partial J}{\partial \mathbf{v}^h}\right]$$

once and computes the derivative from equation (14), making the latter approach favourable for problems with large number of design variables.

The equation

$$\left(\frac{\partial \mathbf{c}}{\partial \mathbf{v}^h}\right)^{T}\lambda^h = \frac{\partial J}{\partial \mathbf{v}^h}^{T}$$

is called the (discrete) adjoint equation.

Remark 3.2. When using the modified Cross model (3), (4), the viscosity μ depends on $\mathbf{u}^h(\boldsymbol{\alpha})$ and on $\mathbf{x}^h(\boldsymbol{\alpha})$. (The dependence on $\mathbf{u}^h(\boldsymbol{\alpha})$ is obvious, the dependence on $\mathbf{x}^h(\boldsymbol{\alpha})$ is due to the fact that the Jacobians of $\mathbf{u}^h(\boldsymbol{\alpha})$ are required (see, e.g. He *et al.* (1997) or Haslinger and Neittaanmäki (1996)).

We have already mentioned in Remark 3.1 that in our computations, the terms involving partial derivatives $\partial\gamma/\partial\mathbf{u}^h$ are dropped from the computation of $\partial\mathbf{c}^h/\partial\mathbf{u}^h$. We also drop terms involving partial derivatives $\partial\gamma/\partial\mathbf{x}^h$ from the computation of $\partial\mathbf{c}^h/\partial\mathbf{x}^h$. Therefore, our computed gradient $\nabla\hat{J}^h(\boldsymbol{\alpha})$ is inexact when using the modified Cross constitutive model.

Table 3. The design variables for the graft optimization for case 2, $Re = 300$.

Design variable	Initial	Newtonian	Modified Cross
r_2	0.0	2.024	1.953
r_3	0.0	− 1.038	− 1.063
r_4	0.0	0.238	0.261
r_5	0.0	− 0.014	− 0.019

Note that we follow the so-called discretize-then-optimize approach, i.e. we first discretize the optimization problem to obtain equation (6) and then we solve the resulting non-linear programming problem (10). Other approaches are possible. We refer to (Stanley and Stewart 2002, Gunzburger 2003, Abraham *et al.* 2004) for more details.

3.3 Mesh sensitivity and adaptation

For the gradient computation we need to compute $\mathrm{d}\mathbf{x}^h/\mathrm{d}\boldsymbol{\alpha}$. We also need a method that given a current design $\boldsymbol{\alpha}$ and a new design $\boldsymbol{\alpha} + \delta\boldsymbol{\alpha}$, computes $\mathbf{x}^h(\boldsymbol{\alpha} + \delta\boldsymbol{\alpha})$ from $\mathbf{x}^h(\boldsymbol{\alpha})$. In our examples, the domains and finite element meshes are simple enough so that we can explicitly determine the map $\boldsymbol{\alpha} \mapsto \mathbf{x}^h(\boldsymbol{\alpha})$. In this case, the tasks specified above are easily realized. For discussions of other cases see, e.g. Mohammadi and Pironneau (2001).

3.4 Optimization algorithm

The conceptual algorithm for the solution of the shape optimization problem is then

1. Initialize design variable $\boldsymbol{\alpha}$ and compute $\mathbf{x}^h(\boldsymbol{\alpha})$.
2. While stopping criteria not satisfied:
   (a) solve $\mathbf{c}(\mathbf{v}^h(\boldsymbol{\alpha}),\mathbf{x}^h(\boldsymbol{\alpha})) = 0$,
   (b) evaluate $\hat{J}^h(\boldsymbol{\alpha}) = J(\mathbf{u}^h(\boldsymbol{\alpha}), p^h(\boldsymbol{\alpha}), x^h(\boldsymbol{\alpha}), \boldsymbol{\alpha})$,
   (c) solve mesh sensitivity equation to get $\mathrm{d}\mathbf{x}^h/\mathrm{d}\boldsymbol{\alpha}$,
   (d) solve adjoint equation,
   (e) compute $\nabla\hat{J}^h(\boldsymbol{\alpha})$,
   (f) use $\nabla\hat{J}^h(\boldsymbol{\alpha})$ to determine design update $\delta\boldsymbol{\alpha}$. Set $\boldsymbol{\alpha} = \boldsymbol{\alpha} + \delta\boldsymbol{\alpha}$,
   (g) adapt the mesh to get $x^h(\boldsymbol{\alpha})$.

In our test cases $\mathcal{A}_{\mathrm{ad}} = \mathbb{R}^n$ and we use a BFGS quasi-Newton method (Dennis and Schnabel 1996, Nocedal and Wright 1999) with line search to solve equation (10). Specifically, we have interfaced our flow code with the optimization code (Spellucci 1998), which can also handle constraints on the design parameters.

4. Numerical results

In all computations, the viscosity for the Newtonian case is chosen to be $\mu = \mu_\infty$, which is what one would have done had the model not been available (Gijsen *et al.* 1999).

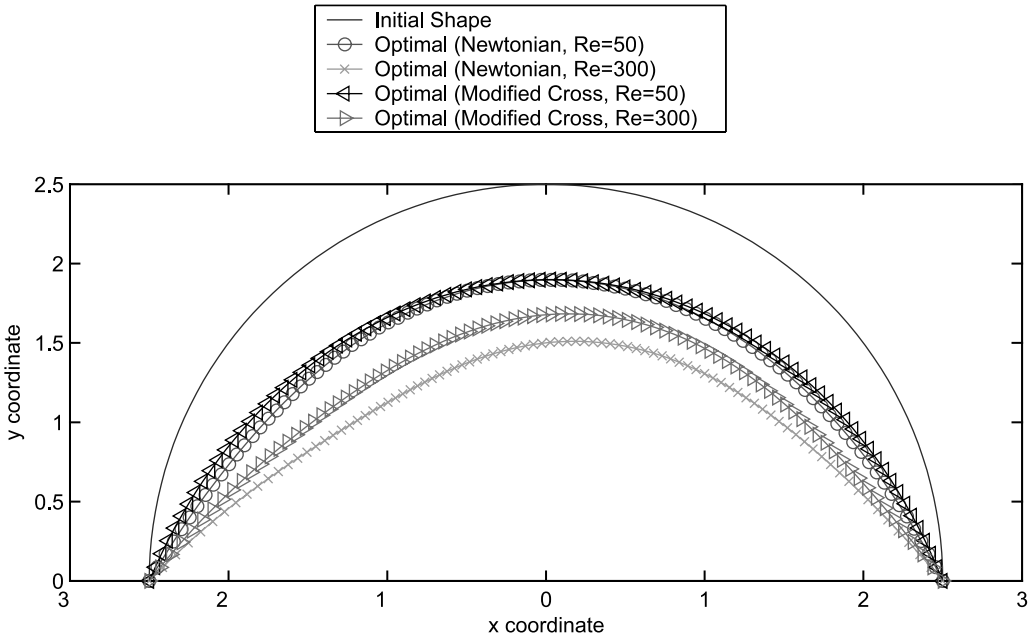

Figure 11. Initial shape and optimal shape of the graft design curve for the Newtonian and modified Cross constitutive model, $d = 1.0$.

The observation region $\Omega(\boldsymbol{\alpha})_{\text{obs}}$ for both the test cases is the entire flow domain.

The optimization algorithm is stopped if the norm of the gradient is less than $\|\nabla\hat{J}(\boldsymbol{\alpha}_0)\| \times 10^{-8}$ for the Newtonian constitutive equations and $\|\nabla\hat{J}(\boldsymbol{\alpha}_0)\| \times 10^{-7}$ for the modified Cross model, where $\nabla\hat{J}(\boldsymbol{\alpha}_0)$ is the gradient at the initial design. The lower choice of the stopping criterion when using the modified Cross model is due to the inexactness of our gradient computation (c.f. Remarks 3.1 and 3.2).

4.1 Arterial grafting

We consider the arterial grafting problem, where a graft is attached upstream of the occlusion in the artery as an alternative route for blood flow (see, e.g. Taylor (2000) and references cited therein). The boundary conditions for the modeled flow field are specified parabolic inlet velocity, no-slip boundary conditions on all walls including the graft, and a parallel flow condition at the outlet. We present results for two different Reynolds numbers 50 and 300, defined as $\rho V_{\max} H/\mu_\infty$, where $H = 0.8$ is the height at the inlet and $V_{\max}$ is the maximum velocity at the inlet. Figure 1 shows the geometry of the problem, with the flow proceeding from left to right. The geometry of the artery (rectangles in figure 1) is fixed. The shape of the graft is optimized.

Table 4. The angle that the graft makes with the artery for case 2.

Angle	Initial	Newtonian	Modified Cross
$\theta = 0$, $Re = 50$	90.00°	63.50°	68.35°
$\theta = \pi$, $Re = 50$	90.00°	59.65°	67.18°
$\theta = 0$, $Re = 300$	90.00°	50.12°	53.32°
$\theta = \pi$, $Re = 300$	90.00°	46.27°	52.24°

We use the parameterization

$$r(\theta) = \sum_{i=0}^{P} r_i \theta^i \tag{15}$$

with $P = 5$, to represent the centerline of the graft.

Two conditions that ensure that location of the connection between graft and artery is fixed are used to express r_0 and r_1 in terms of the other ones. Hence, our design variables $\boldsymbol{\alpha}$ consist of r_i, $i = 2,\ldots, P$.

The mesh in the subdomain representing the artery is fixed. For a given centreline (15), the nodal points $\mathbf{x}^h$ of the triangulation of the graft are obtained by moving in the radial direction from the centreline by a constant distance. This defines the map $\boldsymbol{\alpha} \rightarrowtail \mathbf{x}^h(\boldsymbol{\alpha})$.

4.1.1 Case 1. We define the aspect ratio as the ratio of the diameter d to height H. In the first case, $d = 0.6$ and the aspect ratio is 0.75. The domain is discretized using 3137 triangular elements and 1774 nodes. The shear rate and the corresponding viscosity given by equation (4), are evaluated at the centroid of each element of the discretization, and are plotted in figure 2. For the case when the Reynolds number is 300, the optimization process led to a 14.98% reduction in the dissipation function using the Newtonian constitutive equation, and a 16.38% reduction in the dissipation function using the modified Cross model. The streamline plot of the velocity fields for the initial and optimal shapes for the two constitutive model choices are shown in figures 3 and 4. Figure 5 shows that for an aspect ratio of 0.75 the optimal shapes are independent of the choice of the constitutive model, but vary somewhat with Reynolds number. Table 1 shows the computed optimal shape parameters defined in

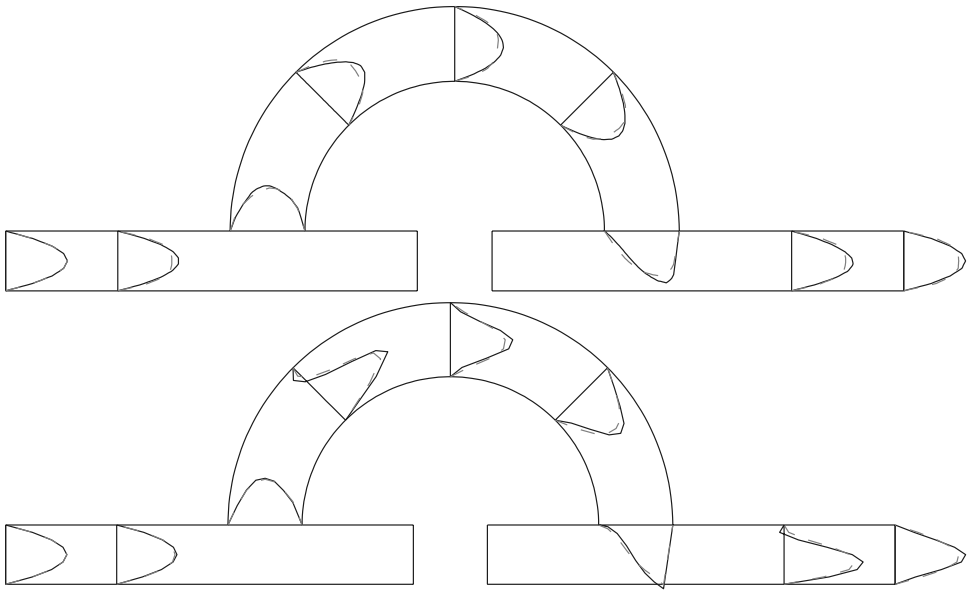

Figure 12. Axial velocity plot at various locations of the initial graft shape, for case 2, with $Re = 50$ (top) and $Re = 300$ (bottom). Solid line represents Newtonian flow and dashed line represents the flow using the modified Cross constitutive model. The velocities in the top subplot are scaled by a factor of 6 relative to the bottom subplot to emphasize differences in downstream velocity profiles.

equation (15), and table 2 shows the values of the angles that the graft makes at the inlet and exit of the artery.

Figure 6 shows that although the axial velocity profiles for the smaller Reynolds number is qualitatively larger, for either Reynolds number the flow profiles are not that different. A similar effect is seen for the optimal shape velocity profiles, as seen in figure 7. Note that for figures 6 and 7, we use a different scaling for the two inflow Reynolds numbers.

4.1.2 Case 2. In the second case, we let $d = 1.0$, and the aspect ratio is 1.25. The domain is discretized using 3643 triangular elements and 2017 nodes. By increasing the diameter d, the local Reynolds number at the bypass graft inlet is reduced and therefore the shear rate is also lowered. The shear rate and the corresponding viscosity given by equation (4), are evaluated at the centroid of each element of the discretization, and are plotted in figure 8. For the case when the Reynolds number is 300, the optimization process gave a 29.0% reduction in the dissipation function using the Newtonian constitutive equation, and a 21.3% reduction in the dissipation function using the modified Cross model. The streamline plot of the velocity fields for the initial and optimal shapes for the two constitutive model choices are shown in figures 9 and 10.

We see from table 3, the numerical differences in the optimal shape parameters defined in equation (15) when

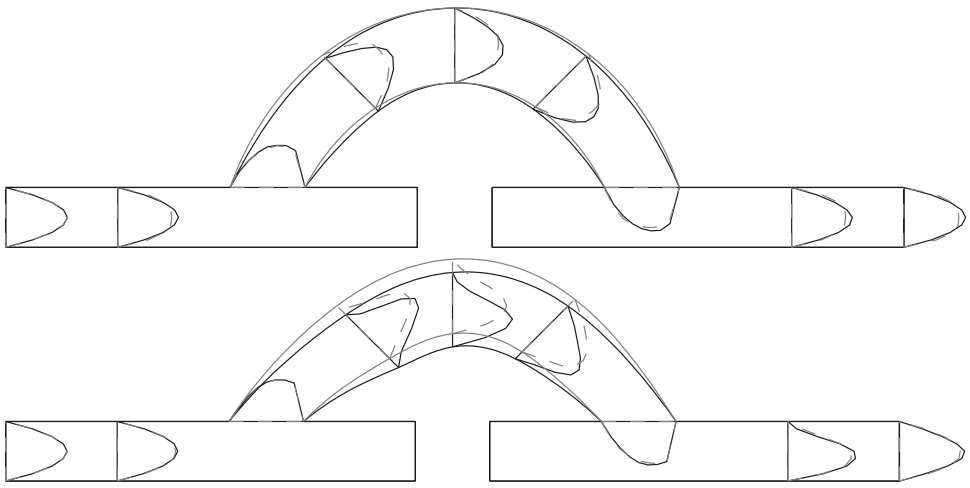

Figure 13. Axial velocity plot at various locations of the optimal graft shapes using each of the constitutive equation (overlapped here), for case 2, with $Re = 50$ (top) and $Re = 300$ (bottom). Solid line represents Newtonian flow and dashed line represents the flow using the modified Cross constitutive model. The velocities in the top subplot are scaled by a factor of 6 relative to the bottom subplot to emphasize differences in downstream velocity profiles.

$Re = 300$. Figure 11 and table 4 show the significant influence of the shear-thinning property on the obtained optimal shape. Specifically, for the higher Reynolds number there is a larger difference in the computed shape. Moreover, the angle that the graft makes with the artery depends significantly on the constitutive equation used, as well as on the Reynolds number. For $Re = 50$ the differences in angles computed with Newtonian and modified Cross constitutive equation, respectively, seem slightly larger than for $Re = 300$.

Figure 12 shows a strong influence of the axial velocity profiles due to the inclusion of the shear-thinning model. We see from figure 13 that due to the difference in the shapes obtained from the choice of the respective constitutive equation, there is a qualitative similarity in the flow profiles in the domain.

5. Conclusions and future directions

We have outlined the solution of shape optimization problems governed by the Navier-Stokes equations with a generalized Newtonian constitutive model. The governing equations are discretized by stabilized finite elements. The resulting optimization problem is solved using a gradient-based method. Our numerical results show the benefits of numerical shape optimization in achieving design improvements.

The choice of constitutive equation did impact the optimal shape in our example—the optimization of an idealized arterial graft. For a smaller aspect ratio, the optimal shapes do not differ much for either choice of Reynolds number. However, when we increased the aspect ratio, the flow profiles significantly differ between the generalized Newtonian constitutive model and the Newtonian one, and the optimal shapes obtained were significantly different. This was especially the case for higher Reynolds number, with dominant flow features such as recirculation more prevalent when using the Newtonian constitutive equation. This suggests that, when considering larger graft-to-artery diameter ratios such as 1.5 and 2.0 in Longest and Kleinstreurer (2003) for the distal end-to-side femoral bypass, the prevalent shear rate would lead to higher differences between the Newtonian and generalized Newtonian treatments. Our results obtained with the modified Cross model are equally applicable for any other shear-thinning model such as the Carreau-Yasuda, Quemada or the Casson model, which exhibit qualitatively similar dependence of the viscosity on the shear rate (see, e.g. Johnston *et al.* (2004) or Neofytou and Drikakis (2003)).

A Newtonian assumption is valid for flows where shear rates are high, thus diminishing the shear-related viscosity differences as seen in equation (3). The objective function employed here, which is relevant for many blood related design objectives, tries to minimize the dissipation function. Thus, our shape optimization tends to select shapes for which also the local shear rate tends to be smaller. In these cases, we expect a stronger influence of the constitutive model on the computed shape.

The optimal shapes obtained herein are limited by the parameterization we admit. A parameterization that accommodates high-order shape variations would be more useful in a realistic scenario, e.g. when considering graft hood shapes obtained in Longest and Kleinstreurer (2003). Our objective function which minimizes the integral of the squared shear rate globally does not prevent undesirable effects on blood cells arising from very low local shear rates such as seen in recirculation and stagnation zones. To overcome this deficiency in our problem setting, a realistic and practical optimization problem might add explicit bound constraints on local shear rates to equation (6). There has been recent interest in developing more clinically useful blood damage measures (see Arora *et al.* (2004) and references cited therein), and it would be worthwhile to extend the use of these measures in the optimization problem.

We are working towards extending our optimal design capabilities to handle simulations involving unsteady 3D pulsatile flows in complex geometries, that make use of more clinically significant objective functions. Such a tool would allow us to, e.g. study the distal placement of the graft and the effect of existing partial stenosis, which allows for prograde or retrograde flows between the ends of the graft, on its placement. The levels of existing stenosis are patient specific, and geometric sensitivity analysis of the effect of stenosis on the placement of the graft could be a useful clinical tool for the clinician in search of a robust surgical procedure.

Acknowledgements

The authors gratefully acknowledge computing resources provided by the NSF MRI award EIA-0116289. This work was supported by the National Science Foundation under award ACI-0121360, CTS-ITR-0312764 and by Texas ATP grant 003604-0011-2001.

References

F. Abraham, "Stabilized finite element solution of optimal control problems in computational fluid dynamics". Ph.D. thesis, Department of Mechanical Engineering and Materials Science, Rice University, 2004.

F. Abraham, M. Behr and M. Heinkenschloss, "The effect of stabilization in finite element methods for the optimal boundary control of the Oseen equations", *Finite Elem. Anal. Des.*, 41, pp. 229–251, 2004.

J.F. Antaki, O. Ghattas, G.W. Burgreen and B. He, "Computational flow optimization of rotary blood pump components", *Artif. Organs*, 19, pp. 608–615, 1995.

D. Arora, M. Behr and M. Pasquali, "A tensor-based measure for estimating blood damage", *Artif. Organs*, 28, pp. 1002–1015, 2004.

M. Behr and D. Arora, "Shear-slip mesh update method: Implementation and applications", *Comput. Methods Biomech. Biomed. Eng.*, 6, pp. 113–123, 2003.

G.W. Burgreen, J.F. Antaki, Z.J. Wu and A.J. Holmes, "Computational fluid dynamics as a development tool for rotary blood pumps", *Artif. Organs*, 25, pp. 336–340, 2001.

J.E. Dennis Jr. and R.B. Schnabel, *Numerical Methods for Nonlinear Equations and Unconstrained Optimization*, Philadelphia: SIAM, 1996.

F.J.H. Gijsen, F.N. van de Vosse and J.D. Janssen, "The influence of the non-Newtonian properties of blood on the flow in large arteries: Steady flow in a carotid bifurcation model", *J. Biomech.*, 32, pp. 601–608, 1999.

V. Girault and P.A. Raviart, *Finite Element Methods for the Navier-Stokes Equations*, New York: Springer-Verlag, 1986.

Y. Grad and S. Einav, "Spectral and instantaneous flow characteristics of vascular junctions using continuous dpiv", *9th International Symposium on Applications of Laser Techniques to Fluid Mechanics*, Lisbon, Portugal, 1998.

M. Grigioni, C. Daniele, U. Morbiducci, G. D'Avenio, G. Di Benedetto, C. Del Gaudio and V. Barbaro, "Computational model of the fluid dynamics of a cannula inserted in a vessel: Incidence of the presence of side holes in blood flow", *J. Biomech.*, 35, pp. 1599–1612, 2002.

M.D. Gunzburger, *Finite Element Methods for Incompressible Viscous Flows: A Guide to Theory, Practice and Algorithms*, Boston: Academic Press, 1989.

M.D. Gunzburger, *Perspectives in Flow Control and Optimization*, Philadelphia: SIAM, 2003.

L. Guo, D. Steinman, B. Moon, W. Wan and R. Millsap, "Effect of distal graft anastomosis site on retrograde perfusion and flow patterns of native coronary vasculature", *Ann. Thorac. Surg.*, 72, pp. 782–787, 2001.

J. Haslinger and P. Neittaanmäki, *Finite Element Approximation for Optimal Shape, Material, and Topology Design*, 2nd ed., Chichester, NY: John Wiley & Sons, 1996.

B. He, O. Ghattas and J.F. Antaki, "Computational strategies for shape optimization of Navier-Stokes flows", Technical Report CMU-CML-97-102 Pittsburgh, FL: Computational Mechanics Lab, Department of Civil and Environmental Engineering, Carnegie Mellon University, 1997.

T.J.R. Hughes, L.P. Franca and G.M. Hulbert, "A new finite element formulation for computational fluid dynamics: VIII. The Galerkin/least-squares method for advective-diffusive equations", *Comput. Methods Appl. Mech. Eng.*, 73, pp. 173–189, 1989.

K. Jansen, S.S. Collis, C. Whiting and F. Shakib, "A better consistency for low-order stabilized finite element methods", *Comput. Methods Appl. Mech. Eng.*, 174, pp. 153–170, 1999.

B. Johnston, P.R. Johnston, S. Corney and D. Kilpatrick, "Non-Newtonian blood flow in human right coronary arteries: Steady state simulations", *J. Biomech.*, 37, pp. 709–720, 2004.

C.T. Kelley, *Iterative Methods for Linear and Nonlinear Equations*, Philadelphia: SIAM, 1995.

A. Leuprecht and K. Perktold, "Computer simulation of non-newtonian effects on blood flow in large arteries", *Comput. Methods Biomech. Biomed. Eng.*, 4, pp. 149–163, 2001.

P.W. Longest and C. Kleinstreurer, "Particle-haemodynamics modeling of the distal end-to-side femoral bypass: Effects of graft caliber and graft-end cut", *Med. Eng. Phys.*, 25, pp. 843–858, 2003.

B. Mohammadi and O. Pironneau, *Applied Shape Optimization for Fluids*, Oxford: Oxford University Press, 2001.

P. Neofytou and D. Drikakis, "Non-Newtonian flow instability in a channel with a sudden expansion", *J. Non-Newtonian Fluid Mech.*, 111, pp. 127–150, 2003.

J. Nocedal and S.J. Wright, *Numerical Optimization*, Berlin/Heidelberg/New York: Springer Verlag, 1999.

K. Perktold, R.O. Peter, M. Resch and G. Langs, "Pulsatile non-Newtonian flow in three-dimensional carotid bifurcation models: A numerical study of flow phenomena under different bifurcation angles", *J. Biomed. Eng.*, 13, pp. 507–515, 1991.

A. Quarteroni and G. Rozza, "Optimal control and shape optimization in aorto-coronaric bypass anastomoses", *Math. Models Methods Appl. Sci. (M3AS)*, 13, pp. 1801–1823, 2003.

A. Quarteroni, M. Tuveri and A. Veneziani, "Computational vascular fluid dynamics: Problems, models and methods", *Comput. Visualization Sci.*, 2, pp. 163–197, 2000.

F. Shakib, "Finite element analysis of the compressible Euler and Navier-Stokes equations". Ph.D. thesis, Department of Mechanical Engineering, Stanford University, 1988.

P. Spellucci, "DONLP2 users guide", Technical report, Fachbereich Mathematik, Technische Universität Darmstadt, 1998, http://www.mathematik.tu-darmstadt.de.

L. Stanley and D. Stewart, *Design sensitivity analysis*, Frontiers in Applied Mathematics, Philadelphia, PA: Society for Industrial and Applied Mathematics (SIAM), 2002.

C.A. Taylor, "Finite element modeling of blood flow: Relevance to atherosclerosis", in *Computational Fluid–Structure Interaction in the Cardiovascular System, Advances in Fluid Mechanics, Vol. 2—Fluid Structure Interaction, Intra and Extracorporeal Cardiovascular Fluid Dynamics*, P. Verdonck and K. Perktold, Eds., Southampton, Boston, MA: WIT Press, 2000, pp. 249–289.

T.E. Tezduyar, M. Behr and J. Liou, "A new strategy for finite element computations involving moving boundaries and interfaces—the deforming-spatial-domain/space-time procedure: I. The concept and the preliminary tests", *Comput. Methods Appl. Mech. Eng.*, 94, pp. 339–351, 1992.

K.K. Yeleswarapu, "Evaluation of continuum models for characterizing the constitutive behavior of blood". Ph.D. thesis, Department of Mechanical Engineering, University of Pittsburgh, 1996.